

Title Page

Nitro-compounds and GHG exhaust emissions of a pilot diesel-ignited ammonia dual-fuel engine under various operating conditions

Run Chen^{1,2}, Tie Li^{1,2*}, Xinran Wang¹, Shuai Huang¹, Xinyi Zhou¹, Shiyan Li¹, Ping Yi^{1,2}

¹ State Key Laboratory of Ocean Engineering, Shanghai Jiao Tong University

² Institute of Power Plants and Automation, Shanghai Jiao Tong University

*Corresponding Address: 800 Dongchuan Rd., Shanghai, PR China, 200240, Tel.: (86)21-3420-8348; E-mail: litie@sjtu.edu.cn

KEYWORDS:

Diesel, ammonia, engine-out emissions, dual fuel, operating conditions.

SYNOPSIS

Ammonia is the most promising green fuel, but few reports on emissions characteristics of ammonia-fueled engines. This study clarifies the effects of ammonia used as a power source on the atmospheric contamination.

ABSTRACT: In the transportation sector, ammonia used as a power source plays a significant role in the scenario of carbon neutralization. However, the engine-out emissions correlations of ammonia-diesel dual-fuel (DF) engines are still unclear, especially the nitro-compounds of great concern and GHG. In this study, the engine-out emissions are evaluated by using a four-cylinder ammonia/diesel DF engine. Various operating conditions consisting of ammonia energy ratio (AER), engine load, and speed were carried out. Unburned NH_3 increases with raising ammonia content but decreases with increasing engine load and speed. The $\text{NO}+\text{NO}_2$ tendency shows a non-linearity trend with increasing ammonia content, while a trade-off correlation is linked to N_2O . The N_2O emission of ammonia engine significantly weakens the beneficial effect of GHG reduction, the 30% and 50% decarbonization targets need at least 40% and 60% ammonia energy without regard to N_2O 's effect, while at least 65% and 80% ammonia energy respectively with considering N_2O . N_2O presents a parabolic-like tendency with AERs. Advanced pilot-diesel injection timing helps to reduce both NH_3 and N_2O , but this effect becomes insignificant as the AER is less than 0.4. A combustion strategy of the rapid heat release and ammonia-governed heat release respectively are revealed.

INTRODUCTION

The 99% of transportation power source is dominated by high-carbon fossil fuels, such as diesel, gasoline, and heavy oil fuel, which are greatly far off the decarbonization requirements, especially for heavy-duty vehicles and ocean-going shipping. The International Maritime Organization (IMO) proposed a target of 30% and 50% lowering carbon emissions by 2030 and 2050 respectively ^[1]. Such an urgent decarbonization mission is widely recognized to be perfectly resolved by using alternative fuels with low/zero carbon.

Many literatures and reports [2-7] have reviewed the potential green fuels. Ammonia is easily to be liquefaction under -33°C @1atm or 0.9MPa@room temperature, which is more convenient compared with LNG and hydrogen. In addition, ammonia with 17.5wt% of hydrogen helps to contribute the clean combustion as a high-efficiency hydrogen carrier. However, the ammonia's weaknesses of higher ignition resistance and lower flame propagation speed are prone to narrow the reliable operating window, leading to either misfire or undesirable engine-out emissions. The worsened exhaust performance is expected to greatly impede ammonia as a power source in internal combustion engines (ICEs) [8-9].

Due to the convenient utilization and accessibility of diesel fuel, many scholars have focused on the pilot diesel-ignited ammonia dual-fuel CI (compression ignition) engines for recent 15 years. Reiter et al. [10-11] used pre-mixed ammonia in a 4-cylinder CI engine and found the indicated thermal efficiency (ITE) decreased proportionally by adding ammonia. Niki et al. [12-14] investigated the low-pressure gaseous ammonia injection utilized in a CI engine. They pointed out that the early diesel injection helped to reduce both unburned NH_3 and N_2O . Recently, Yousef et al. [15-16] found that the thermal De NO_x process helped to decrease NO_x if the ammonia energy share was less than 40%. Zhou and Li et al. [17] compared the low-pressure premixed and high-pressure spray combustion modes of a low-speed marine engine by numerical simulation. Jin et al. [18] optimized the diesel pilot injection strategies in the ammonia dual-fuel engine by numerical simulation and achieved a 14% reduction of CO_2 . As mentioned above, lots of studies have laid concentration on the energy ratio of ammonia and numerical simulation. However, the engine-out emissions of unburned NH_3 and nitrogen oxides (namely nitro-compounds), and CO_2 under different engine operating conditions are still unclear, especially since the correlations between the emissions are absent. Therefore, this study was experimentally conducted by a 4-cylinder

ammonia-diesel dual-fuel engine to give an insight into the engine-out emissions under various operating conditions. Finally, the possible improvements in engine-out emissions are discussed.

EXPERIMENTAL SETUP AND PROCEDURES

Experimental Setup

In this study, the 4-cylinder and turbocharging CI engine modified by adding gaseous ammonia injection was employed. The specification of the engine system was listed in Table 1. An 8-hole fuel injector for each cylinder provided a pressurized diesel to approach the pilot-ignited premixed ammonia combustion. The diesel quantity was measured by the fuel meter (AVL List GmbH, PD735s). The single-point injection of ammonia was used at the intake system in this study. The liquified ammonia was supplied by the cylinder and gasified through the heat exchanger at the downstream ammonia fuel line. The gaseous ammonia was controlled by over 30°C and fine-regulated to about 0.6MPa (abs.) which ensures the stable gaseous ammonia state. A surge tank was used to eliminate the supply pressure oscillation and the mass flow controller (Brooks Instrument LLC, SLA5800 Series) was employed at the terminal of the ammonia fuel line to precisely control the target energy ratio. The intake temperature was set by the intercooler system with an accuracy of $\pm 2^\circ\text{C}$.

Table 1. Specification of the engine

Engine Type	4-cylinder, Turbocharged
Engine configuration	Four-stroke, direction injection
Valves per Cylinder	4
Bore \times Stroke [mm]	95 \times 102
Compression ratio [-]	17.5
Nozzle hole diameter [mm]	0.127
Nozzle number	8
Power @full load [kW]	22.4@1000 rpm
Rated Power [kW]	112@2800 rpm
Displacement [L]	2.89

The in-cylinder pressure was measured by a highly precise piezoelectric pressure sensor (AVL List GmbH, GH15DK) with a crank angle resolution of 0.5°CA. The sensor's thermal sensitivity is less than ±2% in the temperature range of 20°C to 400°C. The signals of intake/exhaust static pressures and temperatures were collected through the engine central controlling system built by Labview. The exhaust gas analyzer (Horiba Ltd., Mexa-one Plus) was applied to sampling and quantitatively measured the conventional engine-out emissions consisting of the total unburned hydrocarbon (THC), NO_x, CO₂, and so on. And the special pollutants, such as the unburned NH₃ and N₂O, etc. were collected by the Fourier-transform infrared gas analyzer (Horiba Ltd., FTX-ONE-CS) with an accuracy of ±1.0%.

Experimental Conditions and Methodology

Table 2 shows the engine operating conditions. The ammonia injected quantities were set to the energy shares in the range of 0% to 90% (namely 0%e to 90%e), aiming to investigate the effects of ammonia on the dual-fuel mode at the 75% load with the diesel injection timing of the maximum break torque (MBT). Also, the sweeping of the diesel injection timing was conducted to investigate the emission characteristics. Under the 80%e condition, the effects of engine load from 50% to 100% on the engine-out emissions were clarified. Due to the possible ammonia misfire caused by the over-lean at high speed, the ammonia energy ratio was set to 60%e to explore the impacts of engine speed on the pollutant emissions of ammonia-diesel dual-fuel mode.

Table 2. Experimental conditions

Experimental Tests	Parameters			
	Diesel Inj. Timing	Ammonia Energy Ratio	Engine Load	Engine Speed
Engine speed [rpm]	1000	1000	1000	800 to 2500
BMEP [MPa]	0.7	0.7	0.5, 0.7, 0.8, 0.9	0.7

Diesel Injection Pressure [MPa]	120	120	120	120
Ammonia energy share [%e]	0, 20, 40, 60, 80, 90	0, 20, 40, 60, 80, 90	80	60
Diesel Injection Timing [°CA aTDC*]	Sweep MBT±4°CA if w/o misfire or CoV>5%	MBT	MBT	MBT

*aTDC: after top dead center

In this study, the apparent heat release rate (AHRR) was derived from the in-cylinder pressure measurement as shown in Eq.(1), where γ is the specific heat ratio calculated based on the two-zone mode. P is the cylinder pressure, V is the cylinder volume, θ is the crank angle.

$$AHRR = \frac{\gamma}{\gamma-1} \cdot P \cdot \frac{dV}{d\theta} + \frac{1}{\gamma-1} \cdot V \cdot \frac{dP}{d\theta} \quad (1)$$

The ammonia energy ratio (AER, e%) was determined by the total heating value of injected ammonia divided by the total heating value of the fuel amount as shown in Eq.(2).

$$AER(e\%) = \frac{Q_{NH_3}}{Q_f} = \frac{m_{NH_3} \cdot LHV_{NH_3}}{m_d LHV_d + m_{NH_3} \cdot LHV_{NH_3}} \quad (2)$$

where Q_{NH_3} is the injected ammonia energy. Q_f is the total fuel energy. m_{NH_3} and m_d is the mass flow of ammonia and diesel respectively. LHV_{NH_3} and LHV_d is the lower heating value of ammonia and diesel. The combustion efficiency (η_c) was calculated by the heat release by the combustion (Q_r) and the total energy of input fuels, as expressed in Eq.(3).

$$\eta_c = \frac{Q_r}{Q_f} \times 100 \quad (3)$$

The stable combustion limits were defined as the either misfire or the correlation of variation (CoV) for indicated mean effective pressure (IMEP) over 5%.

RESULTS AND DISCUSSION

Unburned Ammonia Slip

Figure 1(a) shows the unburned NH_3 slip and unburned loss varied with the AER. The unburned loss was calculated based on the energy of the engine-out emissions, including CO, CO_2 , THC, and unburned NH_3 . There is a share of approximately 8.5% at the unburned loss under the 90%e condition. This is attributed to the higher ammonia content causing the lower flame propagation speed. The laminar burning velocity of ammonia at near stoichiometric condition is only about 10% of methane ^[19]. The low flame speed leads to an increased amount of unburned NH_3 . It should be noticed that the share of unburned NH_3 mass slip to the total NH_3 fuel mass is almost constant (about 10%) for all AERs, as shown in Fig.1(b). This feature is very useful to predict the unburned NH_3 emission as the ammonia content alters but is greatly dependent on the engine chamber design. Reiter et al. ^[11] pointed out that the ammonia combustion efficiency sustains a constant (about 5%) under different AERs and Niki et al. ^[20] also reported a nearly 15% of the unburned NH_3 as increasing the NH_3 flow rate from 0 to 13.3L/min. Theoretically, the unburned NH_3 is considered to produce from the piston crevice and incomplete combustion. In this study, the increase of in-cylinder pressure for the operating conditions (from 0%e to 80%e) at MBT has few impacts on the unburned NH_3 emissions as shown in Fig.1(b), indicating that the unburned NH_3 in the piston crevice seems to unaffected by the cylinder pressure. This result is consistent with that of Ref.[20]. As a consequence, the incomplete combustion including flame quenching and inaccessible regions of the diesel flame mainly contributes to the unburned NH_3 . According to the discussion above, the effects of heat transfer characteristics of NH_3 premixed flame and spatial penetration of diesel flame plumes on the ammonia-diesel dual-fuel mode should be carefully examined further.

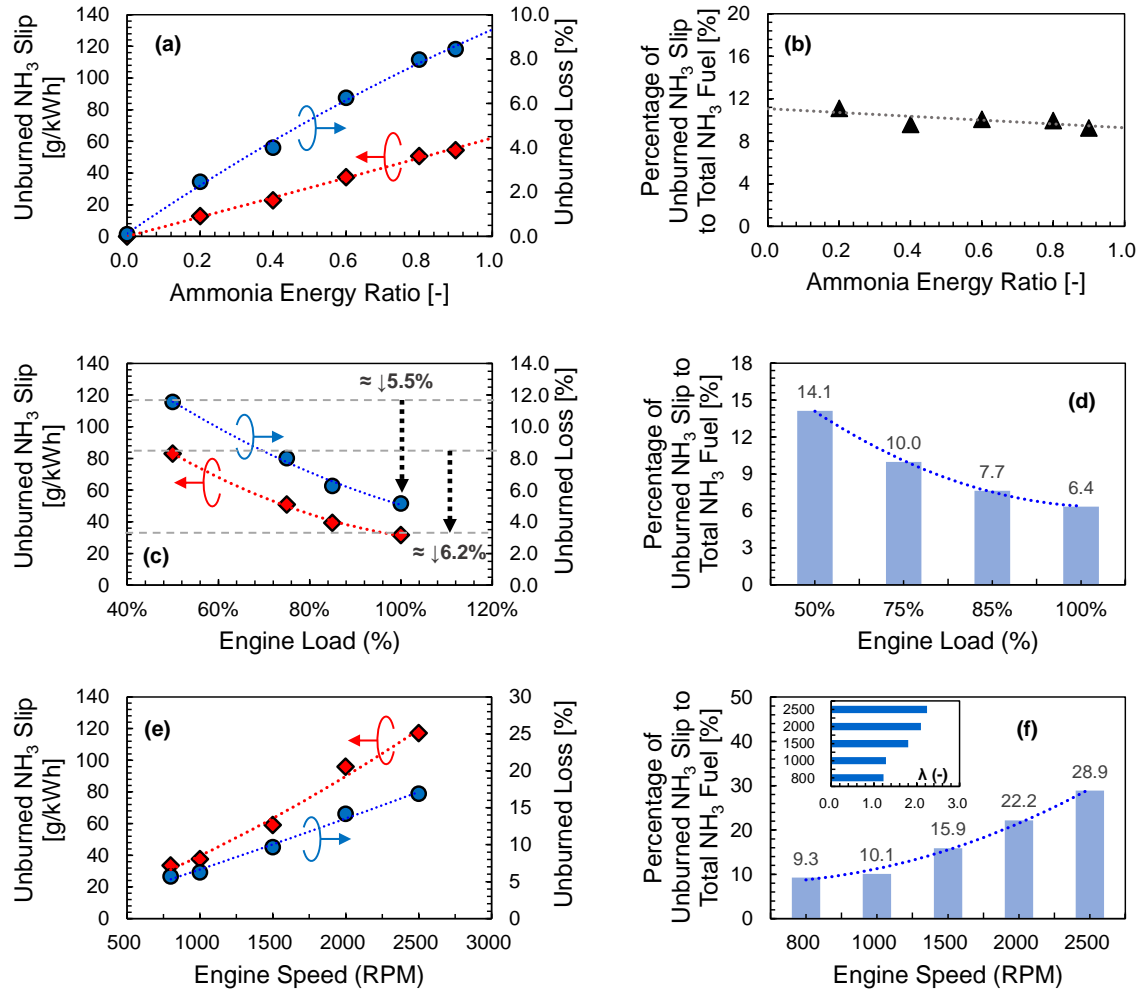


Figure 1. Unburned NH₃ slip characteristics under various operating conditions. (a-b) Unburned NH₃ vs. AER @75% engine load/1000rpm/MBT; (c-d) Unburned NH₃ vs. engine load @80%e/1000rpm/MBT; (e-f) Unburned NH₃ vs. engine speed @80%e/75% engine load/MBT

Figure 1(c) shows the tendencies of unburned NH₃ and unburned loss under different engine loads. The unburned NH₃ decreases by about 6.2% as the engine load increases from 50% to 100%. The higher in-cylinder pressure and temperature under high load promote ammonia decomposition and improve the combustion speed, thus decreasing the unburned NH₃. This facilitation also suggests that 5.5% decrease in the unburned loss from low to high load. Such a tendency indicates that for the ammonia-diesel dual-fuel mode at high AERs, the unburned NH₃ slip nearly determines the total unburned loss.

Under the high engine load, the share of unburned NH_3 to the total NH_3 fuel amount decreases significantly as presented in Fig.1(d). The unburned NH_3 under the low-/mid loads should be taken carefully since these loads are the common operating conditions for ocean-going vessels. Especially the 50% load leads to an over twice increase of the unburned NH_3 share compared with that of 100% load, which might become a great potential challenge for ammonia-power vessels to fitting the future coastal emission control regulations. As shown in Fig.1(e). The unburned NH_3 emission increases about 2.5 times from 800rpm to 2500rpm, as well as the unburned loss rises nearly 12%. The possible reason is attributed to the mixture being lean with increasing engine speed, as shown in Fig.1(f). The mixture becomes over lean ($\lambda = 2.2$ at 2500rpm) at the high speed due to the increase of the air amount. Over lean mixture has a great impact on the ammonia flame quenching during the combustion.

NO_x ($\text{NO}+\text{NO}_2$) Emissions

In Fig.2(a), the NO_x (represented by $\text{NO}+\text{NO}_2$) tendency shows a non-linearity varied with AERs at MBT. When the AER is less than 60%, the NO_x of dual-fuel mode is lower than diesel-only mode, suggesting that the reduction NO_x can be achieved under a lower ammonia energy ratio. From 20%e to 60%e, the NO_x ($\text{NO}+\text{NO}_2$) decreases about 20% compared with that of pure-diesel mode (donated by the blue region). The reduction of $\text{NO}+\text{NO}_2$ under lower AER is attributed to the suppression of thermal NO production by lowering the diesel content and reduced combustion temperature. Nevertheless, when the AER reaches over 60%, the $\text{NO}+\text{NO}_2$ emission amount increases dramatically. At 80%e and 90%e conditions, the $\text{NO}+\text{NO}_2$ emissions show 46% higher than that of the pure-diesel mode. More ammonia content facilitates the increase of HNO from NH_3 pyrolysis, accelerating the important fuel NO route as $\text{HNO} + \text{O}_2 + \text{M} = \text{NO}$. As a result, the

fuel-borne NO trends to become the dominance of NO_x production as the ammonia content approaches a very high level.

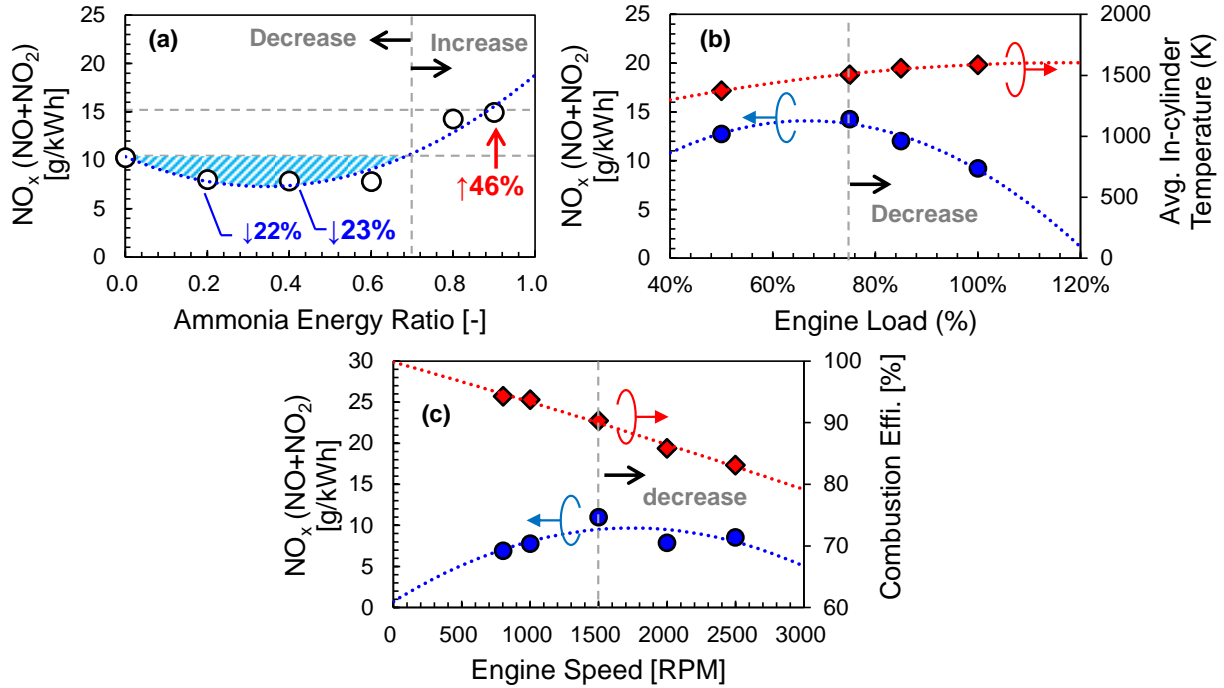


Figure 2. NO_x (NO+NO₂) variation with different operation conditions at MBT. (a) NO_x (NO+NO₂) vs. AER @75% engine load/1000rpm/MBT; (b) NO_x (NO+NO₂) vs. engine load @80%e/1000rpm/MBT; (c) NO_x (NO+NO₂) vs. engine speed @80%e/75% engine load/MBT

Figure 2(b) shows the NO_x (NO+NO₂) tendency varied with different engine loads under 80%e and 1000rpm. The average in-cylinder temperatures derived from SOI to CA90 also are presented. The NO_x emission firstly increases as the engine load rises, but decreases when the load exceeds 80%. As the engine load raises from 40% to 75%, the NO_x increases probably as a result of the thermal NO_x significantly produced due to the in-cylinder temperature rising. Even though the DeNO_x chemistry through the pathways of $\text{NH}_2 + \text{NO} = \text{N}_2 + \text{H}_2\text{O}$ and $\text{NH}_2 + \text{NO} = \text{NNH} + \text{OH}$ is activated from 1100 to 1400K [21-22], the total NO+NO₂ emissions from 40% to 75% load is determined by the balance of local thermal NO_x formation and DeNO_x reactions during combustion. Under the high load condition, however, the NO_x turns to decrease obviously although

the in-cylinder temperature increases steadily. This is possibly attributed to more NH_3 burning under high loads, contributing to acceleration of the thermal DeNO_x . The effects of engine speed on the NO_x emission are exhibited in Fig.2(c). The reduction of combustion efficiency with increasing engine speed suggests that the burning intensity is suppressed by raising speed. In addition, the leaner in-cylinder mixture also promotes reducing the combustion temperature, so that the thermal NO formation is impeded with increasing engine speed.

N_2O Emission

The feature of N_2O 's greenhouse-warming potential (GWP) of 300 times than CO_2 greatly determines the net effect of shipping decarbonization by using ammonia as the power source. Figure 3(a) shows the N_2O variation with AERs, combined with the average in-cylinder temperature. The N_2O increases with the ammonia energy taking up to 60% and then reduces when the AER becomes higher in further. First, the NH_2 radicals from the NH_3 pyrolysis fast dehydrogenated and facilitate the N_2O formation by $\text{NH} + \text{NO} = \text{N}_2\text{O} + \text{H}$ as the temperature is over 1400K [23-24], which is considered as the primary path for N_2O formation [25]. Secondly, Mathieu et al. [26] also pointed out that the N_2O thermal consumption by $\text{N}_2\text{O} + \text{H} = \text{N}_2 + \text{OH}$ started as the ambient temperature was above 1650K. The above reasons lead to the increase of N_2O emissions from 20%e to 60%e. When the AER reaches over 0.8, the N_2O significantly decreases due to the main consumption of N_2O through $\text{N}_2\text{O} + \text{M} = \text{N}_2 + \text{O} + \text{M}$ presenting under lower in-cylinder pressure while the temperature is over 1300K [27]. Although the in-cylinder temperature reduces significantly (below 1400K) at AER=0.9 as highlighted by a red box in Fig.3(a), the N_2O emission maintains a similar level to AER=0.8. The N_2O is reported to be produced through $\text{NH}_2 + \text{NO}_2 = \text{N}_2\text{O} + \text{H}_2\text{O}$ at the lower temperature range of 970 to 1300K [28]. Combined with the above discussion, it indicates that a stagnation of N_2O formation might present

between 1300 to 1400K, possibly leading to a similar level of N₂O emissions for AER=0.8 and 0.9.

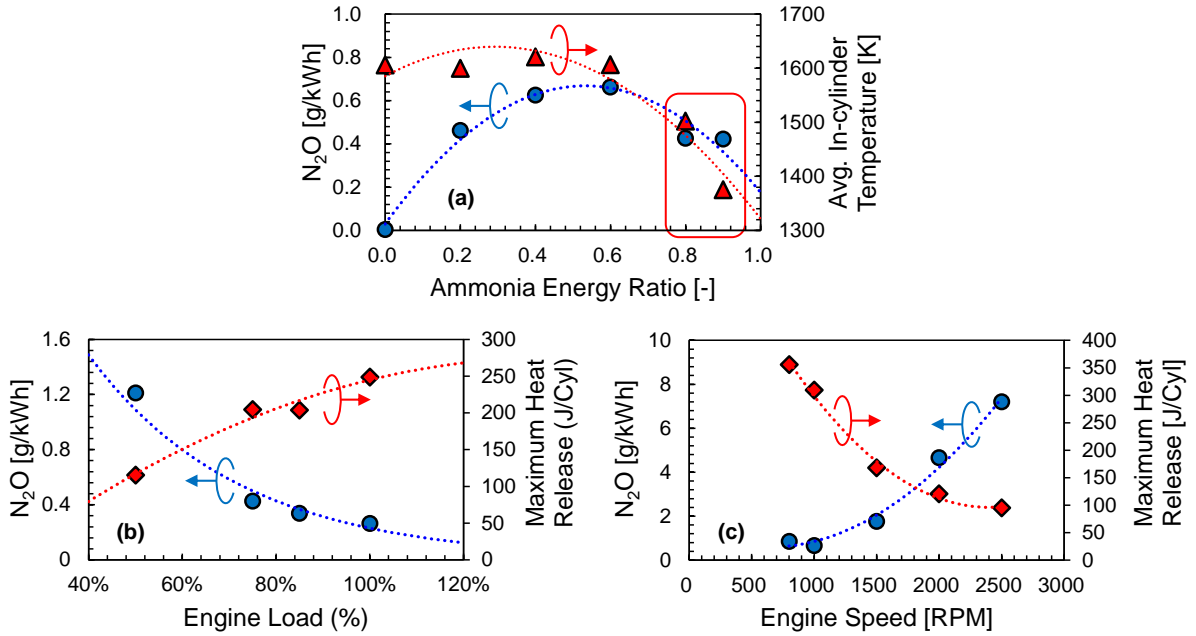


Figure 3. N₂O variation with different operation conditions at MBT. (a) N₂O vs. AER @75% engine load/1000rpm/MBT; (b) N₂O vs. engine load @80%/1000rpm/MBT; (c) N₂O vs. engine speed @80%/75% engine load/MBT.

Figures 3(b) and (c) exhibit the N₂O variation with different engine loads and speeds for AER=0.8 at MBT respectively. Since the in-cylinder temperature and pressure increase at higher engine load conditions, the maximum heat release raises, significantly promoting the N₂O thermal decomposition thus reducing N₂O emissions as shown in Fig.3(b). Moreover, the local leaner mixture as the engine speed increases, leads to a slower flame propagation speed. This impact results in a lower heat release (as shown in Fig.3(c)) but also facilitates N₂O formation under low-temperature conditions [28-29].

CO₂ and CO_{2e} Emissions

Figure 4(a) shows the CO₂ reduction varied with the AER. The equivalent CO₂ emission, namely CO_{2e}, is calculated by the CO₂ emission adding the N₂O amount multiplied by 300 times. The CO₂ reduction comes up to 31% when the AER reaches 0.4, nearly 50% as AER=0.6, without considering the effects of N₂O. Theoretically, the 60% energy share of ammonia in the dual-fuel mode can achieve 50% decarbonization. However, the true carbon reduction is greatly determined by the N₂O emission as a result of N₂O's significant greenhouse effect as shown by a red zone in Fig.4(a). The ammonia energy share has to reach at least 80% to fit the 50% CO₂ reduction, indicating that the decarbonization requirements become more rigorous dramatically if considering the N₂O emission. Due to the peak of N₂O emission occurring at the AER=0.4 to 0.6, therefore, there is an observable decarbonizing weakened region (denoted by red color) at the above conditions, which dramatically narrows the true decarbonization (marked by green color) operating window under different AERs. As a result, the true 50% decarbonization is approached only the ammonia energy share is up to 0.8. As a result, a disruptive technology is needed to solve the problem of high N₂O emission of ammonia engine.

Figure 4(b) shows the CO₂ reduction under different engine loads at AER=0.8 and MBT. There is an absent difference for the direct measurement of CO₂ emission (about 200g/kWh) under various engine loads. As a result, the equivalent CO₂ emission is determined by the N₂O formation. Under the 40% engine load, a large amount of N₂O is produced, probably as a result of relatively low-temperature combustion. This leads to a very high CO_{2e} emission of nearly twice those of other engine loads. In addition, the increased engine speed results in increasing CO_{2e} emission as shown in Fig.4(c), which exhibits a similar trend to the N₂O emission in Fig.4(c).

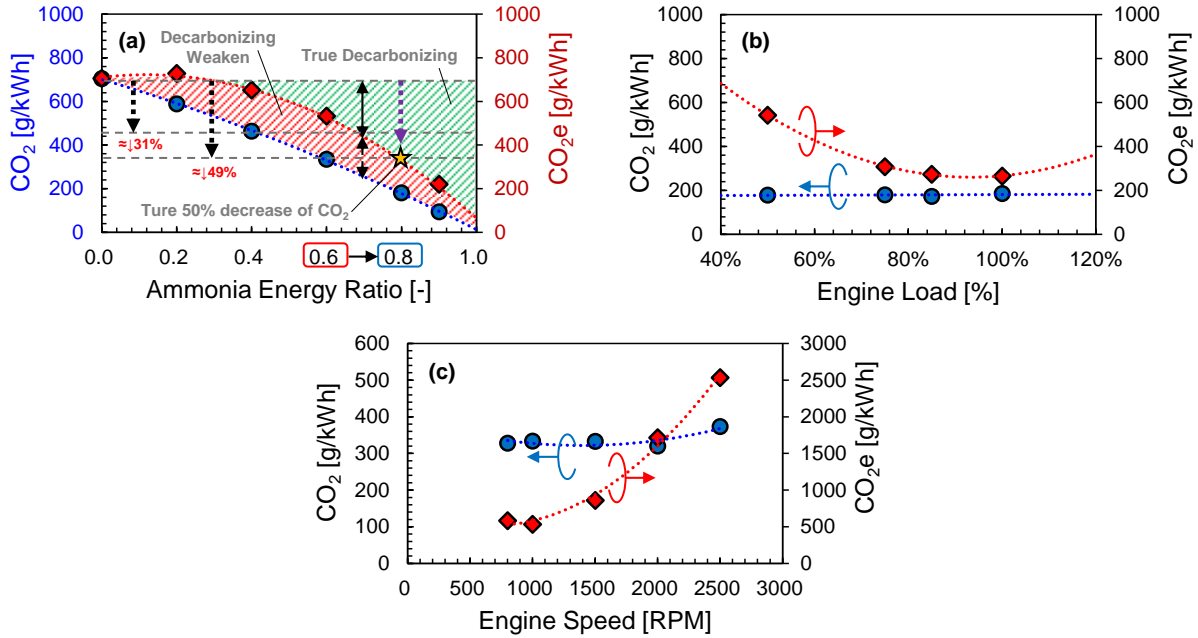


Figure 4. CO₂ variation with different operation conditions at MBT. (a) CO₂ vs. AER @75% engine load/1000rpm/MBT; (b) CO₂ vs. engine load @80%e/1000rpm/MBT; (c) CO₂ vs. engine speed @80%e/75% engine load/MBT.

Combustion Decoupling Characteristics of Ammonia-diesel Duel-fuel Mode

Figure 5 shows the 80%e condition compared with the 20% diesel-only (DO) mode at the same engine speed and engine load. As reported in Ref.[10], the combustion phase shifted advanced if the diesel injection timing is kept the same for the DO mode. To make the comparison more conveniently, the diesel injection timing for the DO mode is retarded by 2 °CA to maintain nearly the same rapid pressure rising with the DF mode. The diesel injection retardation causes about a 1.4% error in the indicated work, which is small enough to be neglected in this study.

In Fig.5(a), the peak of in-cylinder pressure is significantly retarded when the ammonia is introduced into the mixing fuel, due to the ammonia's lower flame speed increasing the ignition delay. And the peak of in-cylinder pressure increases by about 50% of 80%e condition than that of DO mode. The apparent heat release rate (AHRR) of 80%e DF mode can be separated into three periods, namely ignition delay (Start of diesel injection, SOI to CA01), rapid heat release (CA01

to CA50), ammonia-governed heat release (CA50 to CA90) as exhibited in Fig.5(b) to compare with that of the DO mode. After the ignition delay, the AHRR of DF mode rises quickly and reveals a peak of 30% higher than that of DO mode at nearly the same crank angle. The AHRR of the NH₃-only mode can be calculated by the DF AHRR removing that of the DO mode. During the rapid heat release period, the diesel at DO mode almost is burned out, while the ammonia content in DF mode provides about 56% combustion energy suggesting that 1) both the diesel diffusion flame and ammonia premixed combustion are present; and 2) the diesel and ammonia supply the similar level of the heat release during this period at the 80%e condition.

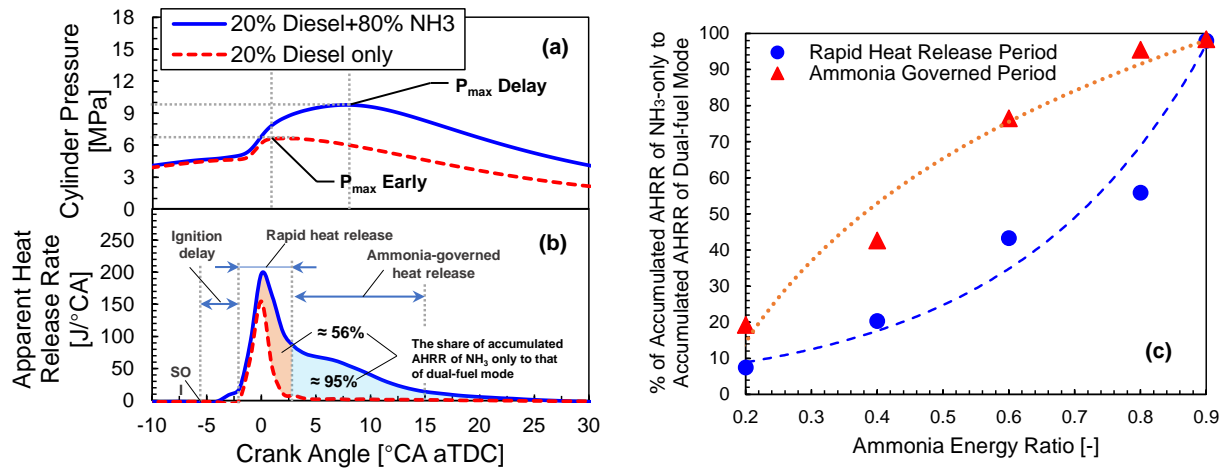


Figure 5. Schematic of combustion decoupling for ammonia-diesel mode. (a-b) Definition of rapid heat release period and ammonia-governed heat release period @80%e/1000rpm/75% engine load/MBT; (c) The tendency of the accumulated AHRR of NH₃-only mode to that of dual-fuel mode @20%e to 90%e/1000rpm/75% engine load/MBT.

After the rapid heat release period, the combustion is almost governed by the ammonia-premixed combustion in the DF mode as shown in Fig.5(b). During this period, premixed ammonia combustion is responsible for about 95% of heat release. This indicates that under higher AER conditions, the method that the proportion of ammonia heat release reduces in the ammonia-governed period while increases in the rapid heat release period may play a very significant role to improve the thermal efficiency and decrease the unburned NH₃.

Figure 5(c) presents the heat release contributions of NH_3 at different combustion periods, which are derived from the percentage of accumulated AHRR of NH_3 -only mode to that of dual-fuel mode. A strong logarithmic relation between the heat release contribution of NH_3 and the ammonia share ratio is observed for the ammonia controlling period, while a significant exponential correlation is found for the rapid heat release period. Under the lower AER conditions, the larger increased rate of NH_3 heat contribution at the ammonia-governed period indicates that the sensitivity of ammonia heat release to the total heat release is more dramatical at the ammonia-governed period. On the opposite, the tendency of NH_3 heat contribution at the rapid heat release period reveals a fact that the NH_3 contribution plays a crucial role under the higher AER conditions during such a period. According to the discussion above, the combustion optimization at the ammonia-governed period for lower AERs, and at the rapid heat release period for higher AERs respectively are in favor of effectively improving the integrated performance of the ammonia-diesel dual-fuel mode.

If the AER raises, the increase of gaseous ammonia volume readily takes up more space in the intake port. This effect greatly decreases the charging efficiency, e.g. the volumetric efficiency reduces by about 18% from AER=0 to 0.9 in this study. The decrease in charging efficiency will deteriorate the thermal efficiency, thus worsening the engine-out emissions. The liquid ammonia with flash-boiling spray^[30] directed into the intake port may play a significant role in the improvement of the volumetric efficiency, as a consequence of the large latent heat of ammonia. However, the wall impingement and interaction with the strong intake crossflow should be carefully examined if using the port injection of liquid ammonia spray.

Figures 6(a) and (b) show the correlation between the unburned NH_3 , N_2O , and NO_x under different AERs and pilot-diesel SOI timings. Similar levels of unburned NH_3 with varied diesel

SOI timing are observed from 20%e to 40%e but show an approximate logarithm relation with N_2O emission from 60%e to 90%e. This tendency indicates that the potential of decreasing both unburned NH_3 and N_2O simultaneously under the very high ammonia condition is possible to be achieved if the pilot-diesel SOI is advanced. But this impact becomes insignificant as the ammonia energy share reduces less than 40%. In addition, a power relation between the NO_x ($NO+NO_2$) and N_2O emissions presents significantly as revealed in Fig.6(b), suggesting the trade-off factor exists between them. The MBT or near MBT positions show the potential to cut down the $NO+NO_2$ and N_2O emissions simultaneously. Moreover, under a certain range of $NO+NO_2$, the emission of N_2O seemingly can maintain a relatively stable level without affecting by the increasing AERs.

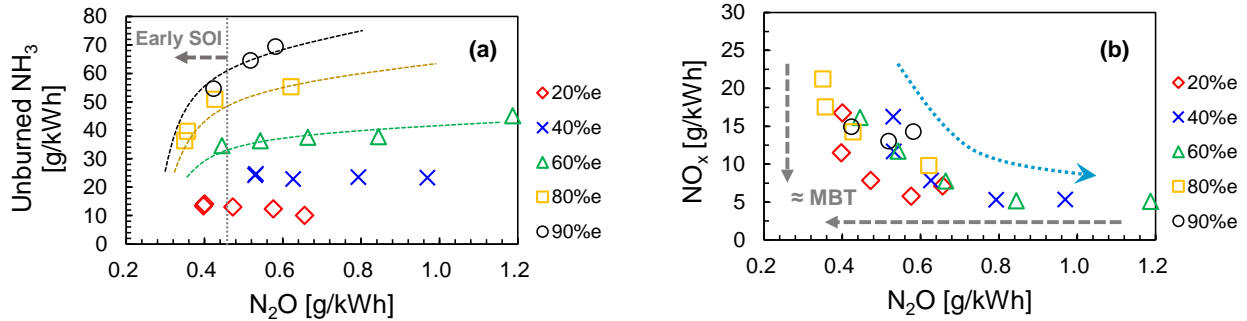


Figure 6. Correlation of N_2O , unburned NH_3 and NO_x under different ammonia energy ratios and diesel SOI timings @1000rpm/75% engine load/MBT.

To lower unburned NH_3 , NO_x as well as N_2O by pilot-diesel injection, the method of firstly holding the target NO_x ($NO+NO_2$), then sweeping the diesel injection timing to find the preferred SOI corresponding to the lower N_2O and unburned NH_3 might be better to acquire the compromised engine-out emissions. The multiple injection strategy integrated with the optimized pilot-diesel injection energy and dwell timing might be expected one of the most efficient ways.

One should be noticed that the N_2O cannot be neglected due to its very significant greenhouse effect which will greatly weaken the integrated decarbonization results, even though the N_2O

emission level is an order of magnitude smaller than that of NO+NO₂ and unburned NH₃. N₂O is produced during the ammonia combustion as well as the late oxidation process of unburned NH₃ from engine crevices during expansion stroke [19, 31-33]. Since the SCR system also will produce a certain level of N₂O, it needs to take into full consideration of the N₂O aftertreatment position coupling with SCR, diesel oxidation catalytic (DOC), and ammonia slip catalyst (ASC). Generally, a disruptive technology is needed to solve the problem of high N₂O emission of ammonia engine.

AUTHOR INFORMATION

Corresponding Author:

*E-mail: litie@sjtu.edu.cn

DECLARATION OF COMPETING INTEREST

The authors declare no competing financial interest.

ACKNOWLEDGMENTS

The authors would like to gratefully acknowledge the support of the Major International (Regional) Joint Research Project of the National Natural Science Foundation of China (52020105009), and the National Natural Science Foundation of China (52271325) and (52171314).

ABBREVIATIONS

AHRR	apparent heat release rate
AER	ammonia energetic ratio
aTDC	after top dead center
ASC	ammonia slip catalytic

BMEP	brake mean effective pressure
°CA	crank angle degree
CI	compression ignition
CA01,50,90	crank angle of 1% / 50% / 90% mass burned fraction
CoV	coefficient of variation
CO _{2e}	equivalent CO ₂ emission
DOC	diesel oxidation catalytic
GHG	greenhouse gas
GWP	global warming potential
ICE	internal combustion engine
IMEP	indicated mean effective pressure
IMO	international Maritime Organization
ITE	indicated thermal efficiency
MBT	maximum brake torque
RAHR	rate of accumulated heat release
SCR	select catalytic reduction
TDC	top dead center

η_c combustion efficiency

W_i indicated work

REFERENCES

- (1) International Maritime Organization (IMO). Adoption of the initial IMO strategy on reduction of GHG emissions from ships and existing IMO activity related to reducing GHG emissions in the shipping sector. IMO Note, 2018.
- (2) Zincir, B.; Deniz, C. An investigation of hydrogen blend fuels applicability on ships. In 2nd International Symposium on Naval Architecture and Maritime. 2014, Istanbul, pp. 23-24.
- (3) Yao, C.; Cheung, C.S.; Cheng, C.; Wang, Y.; Chan, T.L.; Lee, S.C. Effect of diesel/methanol compound combustion on diesel engine combustion and emissions. *Energy Convers. Manag.* 2008, 49(6), 1696-1704.
- (4) Bromberg, L. Benchmarking of alcohol chemical kinetic mechanism for laminar flame speed calculations. 2008.
- (5) Demirbas, A. Methane gas hydrate: as a natural gas source. 2010, Springer, London.
- (6) Heywood, J. B. Internal Combustion Engine Fundamentals, 1998, McGraw-Hill, New York.
- (7) Deniz, C.; Zincir, B. Environmental and economical assessment of alternative marine fuels. *J. Clean. Prod.* 2016, 113, 438-449.
- (8) Zamfirescu, C.; Dincer, I. Using ammonia as a sustainable fuel. *J. Power Sources.* 2008, 185, 459-465.
- (9) Mounaïm-Rousselle, C.; Bréquigny, P.; Medina, A.V.; Boulet, E.; Emberson, D.; Løvås, T. Ammonia as Fuel for Transportation to Mitigate Zero Carbon Impact. In: *Engines and Fuels for Future Transport, Energy, Environment, and Sustainability.* 2022, Springer, Singapore.
- (10) Reiter, A. J.; Kong, S. C. Demonstration of compression-ignition engine combustion using ammonia in reducing greenhouse gas emissions. *Energy Fuels.* 2008, 22(5), 2963-2971.
- (11) Reiter, A. J.; Kong, S. C.; Combustion and emissions characteristics of compression-ignition engine using dual ammonia-diesel fuel. *Fuel.* 2011, 90(1), 87-97.
- (12) Niki, Y.; Yoo, D-H.; Hirata, K.; Sekiguchi, H. Effects of ammonia gas mixed into intake air on combustion and emissions characteristics in diesel engine. In: *Proceedings of the ASME 2016 internal combustion engine fall technical conference.* 2016, NO. 2016-9364.
- (13) Niki, Y.; Nitta, Y.; Sekiguchi, H.; Hirata, K. Emission and combustion characteristics of diesel engine fumigated with ammonia. In: *Proceedings of the ASME 2018 internal combustion engine division fall technical conference.* 2018, NO. 2018-9634.

- (14) Niki, Y. Reductions in unburned ammonia and nitrous oxide emissions from an ammonia-assisted diesel engine with early timing diesel pilot injection. *J. Eng. Gas Turbines Power-Trans. ASME*. 2021, 143(9), 091014.
- (15) Yousef, A.; Guo, H.; Dev, S.; Liko, B.; Lafrance, S. Effects of ammonia energy fraction and diesel injection timing on combustion and emissions of an ammonia/diesel dual fuel engine. *Fuel*. 2022, 314, 122723.
- (16) Yousef, A.; Guo, H.; Dev, S.; Lafrance, S.; Liko, B. A study on split diesel injection on thermal efficiency and emissions of an ammonia/diesel dual-fuel engine. *Fuel*. 2022, 316, 123412.
- (17) Zhou, X.; Li, T.; Wang, N.; Wang, X.; Chen, R.; Li, S. Pilot diesel-ignited ammonia dual fuel low-speed marine engines: A comparative analysis of ammonia premixed and high-pressure spray combustion modes with CFD simulation. *Renew. Sust. Energ. Rev.* 2023. 173, 113108.
- (18) Jin, S.; Wu, B.; Zi, Z.; Yang, P.; Shi, T.; Zhang, J. Effects of fuel injection strategy and ammonia energy ratio on combustion and emission of ammonia-diesel dual-fuel engine. *Fuel*. 2023, 341, 127668.
- (19) Wang, N.; Huang, S.; Zhang, Z.; Li, T.; Yi, P.; Wu, D.; Chen, G. Laminar burning characteristics of ammonia/hydrogen/air mixtures with laser ignition. *Int. J. Hydrog. Energy*. 2021. 46, 31879-31893.
- (20) Niki, Y.; Nitta, Y.; Sekiguchi, H.; Hirata, K. Diesel fuel multiple injection effects on emission characteristics of diesel engine mixed ammonia gas into intake air. *J. Eng. Gas Turbines Power-Trans ASME*. 2019. 141(6), 061020.
- (21) Miller, J.A.; Bowman, C.T. Mechanism and modeling of nitrogen chemistry in combustion. *Prog. Energy Combust. Sci.* 1989. 15(4), 287-338.
- (22) Miller, J.A.; Glarborg, P. Modeling the thermal De-NO_x process: Closing in on a final solution. *Int. J. Chem. Kinet.* 1999. 31(11), 757-837.
- (23) Klippenstein, S.J.; Harding, L.B.; Glarborg, P.; Miller, J.A. The role of NNH in NO formation and control. *Combust Flame*. 2011. 158(4), 774-789.
- (24) Konnov, A.A.; Ruyck, J.D. Kinetic modeling of the thermal decomposition of ammonia. *Combust. Sci. Technol.* 2000. 152(1), 23-37.
- (25) Elbaz, A.M.; Giri, B.R.; Shrestha, K.P.; Arab, O.Z.; Farooq, A.; Mauss, F.; Roberts, W.L. A comprehensive experimental and kinetic modeling study of laminar flame propagation of ammonia blended with propane. *Combust Flame*. 2023. 253, 112791.
- (26) Mathieu, O.; Levacque, A.; Petersen, E.L. Effects of N₂O addition on the ignition of H₂-O₂ mixtures: Experimental and detailed kinetic modeling study. *Int. J. Hydrog. Energy*. 2012. 37(20), 15393-15405.
- (27) Okafor, E.C.; Yamashita, H.; Hayakawa, A.; Somarathne, K.D.K.A.; Kudo, T.; Tsujimura, T.; Uchida, M.; Ito, S.; Kobayashi, H. Flame stability and emissions characteristics of liquid ammonia spray co-fired with methane in a single stage swirl combustor. *Fuel*. 2021, 287, 119433.

- (28) Mendiara, T.; Glarborg, P. Ammonia chemistry in oxy-fuel combustion of methane. *Combust Flame*. 2009. 156(10), 1937-1949.
- (29) Dagaut, P.; Glarborg, P.; Alzueta, M.U. The oxidation of hydrogen cyanide and related chemistry. *Prog. Energy Combust. Sci*. 2008. 34(1), 1-46.
- (30) Li, S.; Li, T.; Wang, N.; Zhou, X.; Chen, R.; Yi, P. An investigation on near-field and far-field characteristics of superheated ammonia spray. *Fuel*. 2022, 324, 124683.
- (31) Tornatore, C.; Marchitto, L.; Sabia, P.; Joannon, M.D. Ammonia as green fuel in internal combustion engines: State-of-the-art and future perspectives. *Front. Mech. Eng*. 2022. 8, 944201.
- (32) Liu, J. Numerical investigation of a heavy-duty CI engine converted to ammonia SI operation. *J. Eng. Gas Turbines Power-Trans ASME*. 2023. 1-41.
- (33) Li, T.; Zhou, X.; Wang, N.; Wang, X.; Chen, R.; Li, S.; Yi, P. A comparison between low- and high-pressure injection dual-fuel modes of diesel-pilot-ignition ammonia combustion engines. *J. Energy Inst*. 2022. 102, 362-373.